ELSEVIER

International Journal of Mass Spectrometry 184 (1999) 153–173

International Journal of Mass Spectrometry

Magnesium chemistry in the gas phase: calculated thermodynamic properties and experimental ion chemistry in H_2–O_2–N_2 flames

QingFeng Chen, Rebecca K. Milburn, Alan C. Hopkinson, Diethard K. Bohme, John M. Goodings*

Department of Chemistry, York University, 4700 Keele Street, Toronto, Ontario M3J 1P3, Canada

Received 18 September 1998; accepted 22 December 1998

Abstract

Molecular orbital calculations were carried out for the neutral and ionic species that occur in the gas-phase chemistry of magnesium in the presence of oxygen and hydrogen including Mg^+, MgO, MgOH, $MgOH^+$, $MgOH_2^+$, $Mg(OH)_2$, $HOMgOH_2^+$, and the hydrate structure $MgOH^+ \ldots (OH_2)$. Standard enthalpies of formation for these species were obtained from single-point calculations at the QCISD(T)(full)/6-311++G(2df,p) and CCSD(T)(full)/6-311++G(2df,p) levels of theory using geometrical parameters obtained from MP2(full)/6-311++G(d,p) optimizations. These ΔH_f^0 values provide a recommended and self-consistent set with uncertainties as small as ± 12.6 kJ mol^{-1} *(± 3 kcal mol^{-1})* for deriving thermodynamic properties. The properties of interest include the proton affinities PA_{298}^0 of MgO, MgOH, and $Mg(OH)_2$, ionization energy IE_0^0 of MgOH, bond dissociation energies D_0^0 of Mg–O, Mg–OH, MgO–H, HOMg–OH, Mg–OH^+, H_2O–Mg^+, and H_2O–$MgOH^+$; the latter two are hydration energies. Values in the literature, both experimental and theoretical, for many of these quantities show considerable scatter and a detailed comparison is made. Magnesium ions in fuel-rich, H_2–O_2–N_2 flames at atmospheric pressure in the temperature range 1820–2400 K were investigated experimentally by sampling the flames doped with magnesium through a nozzle into a mass spectrometer. It was shown that the interconversion of Mg^+ and $MgOH^+$ proceeds by way of the three-body reaction of Mg^+ with OH, in support of Sugden's criterion that this occurs in flames if the weak HO–Mg^+ bond has a dissociation energy less than 335 kJ mol^{-1}. The proton affinity PA_{298}^0(MgO) was measured to be 1056 ± 29 kJ mol^{-1} *(252 ± 7 kcal mol^{-1})* along with approximate values for PA_{298}^0(MgOH) = 919 kJ mol^{-1} *(220 kcal mol^{-1})* and $PA_{298}^0[Mg(OH)_2]$ = 878 kJ mol^{-1} *(210 kcal mol^{-1})*. Values were estimated for the electron–ion recombination coefficient for $MgH_mO_n^+$ molecular ions of 2×10^{-7} cm^3 molecule^{-1} s^{-1}, and for Mg^+ of $4 \times 10^{-24}\ T^{-1}$ cm^6 molecule^{-2} s^{-1} similar to those for alkali metal ions. Finally, small rate coefficients for the chemi-ionization of magnesium via the reactions of Mg + OH and MgO + H to give $MgOH^+$ were estimated to be 4.832×10^{-9} exp($-55\ 700/T$) and 3.341×10^{-9} exp($-32\ 970/T$) cm^3 molecule^{-1} s^{-1}, respectively. (Int J Mass Spectrom 184 (1999) 153–173) © 1999 Elsevier Science B.V.

Keywords: Magnesium; Gas phase; Thermodynamic properties; Flame ion chemistry; Mass spectrometry

* Corresponding author. E-mail: goodings@turing.sci.yorku.ca

PII S1387-3806(99)00002-0

1. Introduction

For many years, it has been known that the addition of alkaline earth metals to hydrogen–oxygen flames produces relatively high levels of ionization [1], the level progressively increasing for Ca, Sr, and Ba. The processes responsible are the two indistinguishable chemi-ionization reactions A + OH and AO + H giving AOH^+ and free electrons e^-, where A is the metal atom [2]. To date, the chemical kinetics have been investigated for Ca, Sr [3,4], and Ba [5]. These studies were performed by sampling a flame doped with an alkaline earth metal through a nozzle into a mass spectrometer. Partly for reasons of completeness, it was decided to study the ion chemistry of magnesium in similar H_2–O_2–N_2 flames that contain only a low level of natural ionization. As a more practical consideration, magnesium combustion is the basis of a vast range of pyrotechnic devices with many civilian and military applications to signal flares, temporary area lighting, etc. in addition to fireworks. From preliminary studies, it is known that magnesium behaves rather differently in flames from the other alkaline earth metals. The degree of ionization is smaller and the dominant ion is Mg^+ and not $MgOH^+$ [6], unlike the other alkaline earths where the $[AOH^+]/[A^+]$ ion ratio is very large for Ba [5] and progressively decreases but only slightly for Sr and Ca [3,5].

An examination of the literature quickly reveals that published thermodynamic values for magnesium of bond strengths, enthalpies of formation, proton affinities and ionization energies are uncertain and, in some cases, differ widely. Accordingly, ab initio calculations were carried out for all the gaseous magnesium species present in flames, which include the neutral oxide and hydroxides as well as the ionic atom, hydroxide, and their hydrates. The results of these calculations are a major help in assessing the validity of experimental values and in providing seemingly reasonable values for quantities that have not been measured experimentally.

The alkaline earth metals exist in flames primarily as neutral species which include atomic A, but also the compounds AO, AOH, and $A(OH)_2$; in most cases, the hydroxides are the dominant neutrals [6,7]. In general, it can be safely assumed that the total concentration of metallic ions is small compared to the total concentration of metallic neutrals; a small addition of Ba is exceptional because the degree of ionization is high [5]. Small hydrate ion signals are observed for all of these metals as members of the two series $A^+.nH_2O$ and $AOH^+.nH_2O$ ($n = 0, 1, 2, \ldots$). Because water is such a major combustion product downstream in these flames, most of the hydrate signals do not represent genuine flame ions. They arise because of the cooling that occurs during sampling of the flame through the nozzle; the hydration equilibrium shifts in the exothermic direction to enhance the hydrates compared with the A^+ or AOH^+ parent ion signals. However, fast proton transfer from H_3O^+, the predominant natural flame ion, can be a major source of the same metallic ions by chemical ionization (CI) of metallic neutral species. The hydrate ions with n = 1 can be interpreted as protonated forms of the dominant hydroxide neutrals; e.g. $A^+.H_2O = AOH.H^+$ (or AOH_2^+) and $AOH^+.H_2O = A(OH)_2.H^+$ (or $HOAOH_2^+$) [6]. Thus, it may be incorrect to say that a sampling artefact is entirely responsible for the hydrate ion signals observed with the mass spectrometer. The related thermodynamic quantities of obvious interest are the proton affinities. These include $PA^0_{298}(MgO)$ forming $MgOH^+$ measured previously [8–10], and also PA values for MgOH and $Mg(OH)_2$, which can be obtained from the corresponding hydrate ion signals.

Another point of interest is the formation of the monohydroxide from the atom. This can occur in flames by way of an equilibrated two-body process, $A + H_2O = AOH + H$, or a three-body process, $A + OH + M = AOH + M$, where M is a third body. Exactly the same two reactions are relevant for the interconversion of the ions A^+ and AOH^+. There is a criterion formulated by Sugden [11], then refined but complicated by Jensen [12] with recent measurements by Hayhurst and co-workers [13,14] to the effect that the two-body reaction occurs provided the HO–A or HO–A^+ bond strength exceeds a certain critical value, originally estimated to be 335 kJ mol^{-1} for neutral species [11]; if less than this, the three-

body reaction is favoured. Basically two values of D_0^0(HO–Mg^+) are promulgated in the literature; about 316 [9,10] and 342 kJ mol^{-1} in the JANAF Tables [15]. In either case, the Mg^+ ion is a possible candidate for the three-body reaction; this has recently been shown to be the situation for copper [14]. Another borderline case occurs for neutral Mg where D_0^0(Mg–OH) has been measured in the range 234–347 kJ mol^{-1} [9,10,15–17].

The objectives of this study were twofold, one theoretical and one experimental. Theoretical ab initio calculations of Mg^+, MgO, MgOH, $MgOH^+$, $MgOH_2^+$, $Mg(OH)_2$, and $HOMgOH_2^+$ can yield standard enthalpies of formation with uncertainties as small as $\pm$12.6 kJ mol^{-1} *($\pm$3 kcal mol^{-1})* from which proton affinities, bond energies, and ionization energies can be determined. The aim was to clarify some of the disparate values in the literature. The calculations also provide molecular structures as well as rotational and vibrational temperatures for statistical mechanical calculations of thermodynamic quantities at flame temperatures. From observations of magnesium ions under a variety of flame conditions, the experimental objectives of this study were (1) to ascertain whether the two- or three-body process is operative linking Mg^+ and $MgOH^+$, (2) to measure the proton affinities of MgO, MgOH, and $Mg(OH)_2$, (3) to measure at least a global electron–ion recombination coefficient for magnesium ions with e^-, and (4) to estimate the rate coefficient for chemi-ionization of Mg + OH and/or MgO + H.

2. Ab initio calculations of magnesium species

2.1. Computational methods

All calculations were performed using the GAUSSIAN 94 program [18]. Geometries were optimized using gradient techniques [19,20] at MP2(full)/6-311++G(d,p) [21–27] for all the molecules and ions studied. The optimized structures were characterized by harmonic frequency calculations and shown to be at minima. The frequency calculations also yielded both zero-point energies and the thermal corrections required to calculate the enthalpies at 298.15 K. The zero-point energies from the harmonic frequency calculations were scaled by 0.94 [28]. Single-point calculations were performed at the QCISD(T) level [29] with a basis set of 6-311++G(2df,p) [30] using the geometries optimized at MP2(full)/6-311++G(d,p). Using Pople's notation, this is denoted as QCISD(T)/6-311++G(2df,p)//MP2(full)/6-311++G(d,p), which we abbreviate to QCI. Similarly, single point calculations at the CCSD(T) level [31–34] were also performed with the same 6-311++G(2df,p) basis set using geometries optimized at the MP2(full)/6-311++G(d,p), and we abbreviate this to CCSD. The total energies, ground state configurations, scaled zero-point values and thermal corrections from these calculations are given in Table 1. Structural details are illustrated in Fig. 1. The vibrational and rotational values obtained from the frequency analysis are given in Table 2.

2.2. Energetics

The values given in Table 1 provide the basis for the calculation of standard enthalpies of formation for all of the magnesium species at 0 or 298.15 K. These are given in Table 3 for the MP2, QCI, and CCSD calculations for comparison with experimental values appearing in the literature. To facilitate the comparison, all values in the table are given specifically in kcal mol^{-1} at 298.15 K, i.e. $\Delta H_{f,298}^0$. Three literature sources are considered: the first two are the standard evaluated compilations by Lias et al. [35] and the JANAF Tables [15], and the third is a paper by Freiser's group [9], with which our calculations show a fair measure of agreement. Some of the calculations are in considerable disagreement with the values appearing in the two compilations. Our past experience with similar calculations on other chemical systems where comparison with experiment is possible [36–39] indicates that these calculations provide values with uncertainties of *$\pm$3 kcal mol^{-1}*. In particular, the highest-level coupled cluster CCSD calculations will produce the most reliable values. It is for this reason that the CCSD values are favoured in

Table 1
Total energies (hartrees), zero-point and thermal energies from structural optimizations

Species	MP2[a] (hartrees)[b]	ZPE[c] (kJ mol^{-1}) *(kcal mol^{-1})*	Thermal[d] (kJ mol^{-1}) *(kcal mol^{-1})*	QCI[e] (hartrees)	CCSD[f] (hartrees)
Mg (^1S)	−199.757 39	···	···	−199.773 68	−199.773 64
Mg^+ (^2S)	−199.491 46	···	···	−199.495 97	−199.495 94
MgO ($^1\Sigma^+$)	−274.794 48	5.4	6.3	−274.855 11	−274.852 44
		1.3	*1.5*		
MgOH ($^2\Sigma$)	−275.477 82	28.9	9.6	−275.541 26	−275.540 58
		6.9	*2.3*		
$MgOH^+$ ($^1\Sigma$)	−275.207 54	28.5	9.2	−275.271 08	−275.270 66
		6.8	*2.2*		
$MgOH_2^+$ (C_s)	−275.836 93	59.8	9.6	−275.894 10	−275.893 75
		14.3	*2.3*		
$Mg(OH)_2$ (C_2)	−351.249 45	59.0	16.3	−351.366 91	−351.366 17
		14.1	*3.9*		
$HOMgOH_2^+$ (C_{2v})	−351.586 52	92.0	16.3	−351.701 08	−351.700 51
		22.0	*3.9*		
$MgOH^+ \ldots (OH_2)$[g] (C_s)	−351.521 43	98.7	15.5	···	···
		23.6	*3.7*		
H (^2S)	−0.499 82	···	···	−0.499 82	−0.499 82
H_2 ($^1\Sigma_g^+$)	−1.160 30	···	···	−1.168 36	−1.168 36
O (^3P)	−74.941 47	···	···	−74.990 05	−74.990 00

[a] Optimization at MP2(full)/6-311++G(d,p).
[b] 1 Hartree = 2625.5001 kJ mol^{-1} = *627.50959 kcal mol^{-1}*.
[c] Zero-point energies are scaled by 0.94.
[d] The thermal energy corrections are added to convert the values from 0 to 298.15 K.
[e] Single-point at QCISD(T)(full)/6-311++G(2df,p)//MP2(full)/6-311++G(d,p).
[f] Single-point at CCSD(T)(full)/6-311++G(2df,p)//MP2(full)/6-311++G(d,p).
[g] $MgOH^+ \ldots (OH_2)$ is 178 kJ mol^{-1} *(42.5 kcal mol^{-1})* above $HOMgOH_2^+$; this value is based on the MP2(full)/6-311++G(d,p) calculation at 0 K.

the final column of recommended values in Table 3. Those for MgO, MgOH, and $MgOH^+$ are in good agreement with the experimental values of Operti et al. [9]; their fourth value for $MgOH_2^+$, where the agreement is not as good, is only a rough estimate. Of course, $\Delta H^0_{f,298}$(Mg) is not calculated because it is the reference base to which the other calculated values are anchored. The recommended value for $\Delta H^0_{f,298}(Mg^+)$ is the spectroscopic value with which our QCI and CCSD numbers are in good agreement. Thus, with two exceptions, the CCSD calculations form the basis of the recommended values in Table 3, which are employed subsequently for the derivation of secondary thermodynamic quantities and quantification of the experimental flame data, where required.

The recommended standard enthalpies of formation are expanded in Table 4 to include $\Delta H^0_{f,0}$ and $\Delta H^0_{f,298}$ at the two standard temperatures of 0 and 298.15 K in both kJ mol^{-1} and *kcal mol^{-1}* making use of the thermal energy corrections given in Table 1. This facilitates the derivation of proton affinities (commonly quoted at 298.15 K), bond dissociation, and ionization energies (quoted at 0 K) and enthalpies of hydration (both 0 and 298.15 K are employed).

2.3. Structural details and frequencies

Calculations with MP2(full)/6-311++G(d,p) optimizations provide the geometrical parameters given in Fig. 1 for all the molecules and molecular ions containing magnesium. It is noteworthy that both MgOH and $MgOH^+$ are linear structures and that removal of an electron from MgOH results in a considerable shortening of the Mg–O distance (by

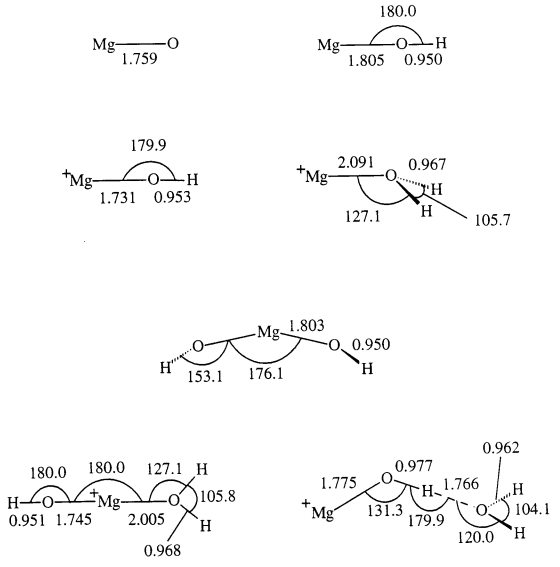

Fig. 1. Geometrical parameters from MP2(full)/6-311++G(d,p) optimizations. The bond lengths are given in angstroms and bond angles in degrees.

0.074 Å) but a small lengthening of the O–H distance (by 0.003 Å). Conversely, protonation of MgOH on O results in elongation of the Mg–O distance (by 0.286 Å), indicating a much weaker bond consistent with the bond energies derived later on in Table 5. The dihydroxide $Mg(OH)_2$ is close to linear at Mg but is nonlinear at O, and the overall structure belongs to the C_2 point group (dihedral angle between the two terminal H atoms is 118.4°). Protonation of $Mg(OH)_2$ on O results in lengthening the Mg–O distance involving the protonated oxygen by 0.192 Å, while the other Mg–O distance decreases by 0.058 Å. The resulting structure has similar Mg–O distances to those in $MgOH^+$ and in $MgOH_2^+$. Of considerable interest is the secondary structure found for $HOMgOH_2^+$ as a true hydrate of $MgOH^+$ represented by $MgOH^+ \ldots (OH_2)$. Based solely on the MP2 calculation at 0 K, it occurs at an energy 178 kJ mol^{-1} *(42.5 kcal* mol^{-1}*)* above the base structure.

Characterising the structures from the MP2 calculations provides rotational and vibrational frequencies, which are given in Table 2, as the equivalent characteristic temperatures in K because they are easier to use in statistical mechanical calculations. In this context, a word of caution is necessary. The vibrational frequencies are derived by fitting harmonic potentials to normal vibrational modes. For shallow potentials where the asymmetry of the well is emphasized, a considerable error in the frequency might result. Thus, the vibrational frequencies given in Table 2 are not intended for the prediction of infrared spectra. The same is true of the rotational frequencies for the prediction of microwave spectra. However, these characteristic temperatures are entirely adequate for statistical mechanical calculations of thermodynamic functions where the logarithm of the partition function is involved. This is particularly applicable to Sec. 3 since thermodynamic quantities

Table 2
Rotational and vibrational temperatures for statistical mechanical calculations

Species	Rotational temperatures (K)[a]	Vibrational temperatures (K)[b]
MgO ($^1\Sigma^+$)	0.817 33	1430.22
MgOH ($^2\Sigma$)	0.686 38 (linear)	251.80, 251.80, 1049.73, 5877.35
$MgOH^+$ ($^1\Sigma$)	0.742 75 (linear)	201.56, 201.56, 1261.62, 5827.04
$MgOH_2^+$ (C_s)	0.488 44, 0.500 51, 20.259 04	517.08, 541.45, 749.46, 2412.06, 5463.98, 5594.61
$Mg(OH)_2$ (C_2)	0.205 00, 0.205 03, 71.835 17	158.86, 243.35, 245.76, 255.39, 293.32, 853.77, 1274.67, 5864.59, 5865.07
$HOMgOH_2^+$ (C_{2v})	0.180 67, 0.182 30, 20.194 44	93.23, 105.18, 305.87, 359.86, 576.61, 607.42, 896.57, 1264.99, 2437.18, 5461.45, 5572.47, 5855.13

[a] The rotational constants (in Ghz) are obtained by multiplying the rotational temperatures by 20.836 74.
[b] The vibrational frequencies (in cm^{-1}) are obtained by dividing the vibrational temperatures by 1.438 786.

Table 3
Comparison of standard enthalpies of formation $\Delta H^0_{f,298}$ at 298.15 K in kcal mol^{-1}

Species	Calculated values (this work)			Experimental literature values			Recommended values[d]
	MP2[a]	QCI[b]	CCSD[c]	Lias et al. [35]	JANAF [15]	Operti et al. [9]	
Mg (^1S)	···	···	···	*35.3*	*35.2 ± 0.2*	···	*35.2*
Mg^+ (^2S)	*210.7*	*213.0*	*213.0*	*211.6*	*211.5 ± 0.3*[f]	···	*211.5*
MgO ($^1\Sigma^+$)	*26.3*	*34.0*	*35.7*	*13.4*	*13.9 ± 6.0*	*36 ± 5*	*35.7*
MgOH ($^2\Sigma$)	*−31.8*	*−25.8*	*−25.4*	*−30*	*−39.4 ± 9.0*	*−22 ± 8*	*−25.4*
$MgOH^+$ ($^1\Sigma$)	*137.6*	*143.5*	*143.7*	*143*[e]	*138.2 ± 15.0*[f]	*146 ± 5*	*143.7*
$MgOH_2^+$ (C_s)	*114.5*	*124.4*	*124.6*	···	···	*∼96*	*124.6*
$Mg(OH)_2$ (C_2)	*−139.1*	*−126.5*	*−126.1*	···	*−136.8 ± 8.0*	···	*−126.1*
$HOMgOH_2^+$ (C_{2v})	*21.6*	*36.1*	*36.4*	···	···	···	*36.4*
$MgOH^+ \ldots (OH_2)$[g] (C_s)	*63.9*	···	···	···	···	···	···

[a] Refer to footnote a of Table 1.
[b] Refer to footnote e of Table 1.
[c] Refer to footnote f of Table 1.
[d] Except for Mg and Mg^+, the recommended values have an uncertainty of ±12.6 kJ mol^{-1} *(±3 kcal mol^{-1}).*
[e] This value refers to Murad's data [10] at 0 K.
[f] For the electron e^-, the JANAF Tables [15] employs the electron (thermal or thermodynamicists') convention whereas all the other data in Table 3 are given in terms of the ion (stationary electron) convention. For comparison of the Mg^+ and $MgOH^+$ values in Table 3, the JANAF values have been converted to the ion convention by subtracting *1.481 kcal mol^{-1}*. The distinction is explained in the introduction to Lias et al. [35].
[g] Refer to footnote g of Table 1.

measured at an average flame temperature of 2100 K have to be transformed to values at the standard temperatures of 0 or 298.15 K.

2.4. Thermodynamic quantities derived from the calculations

Proton affinities, ionization energies, and dissociation energies, some of which are also interpretable as enthalpies of hydration, are presented in Table 5 based on the recommended standard enthalpies of formation given in Table 4. These values based on the CCSD calculations are compared with experimental (and a few other theoretical) numbers available in the literature, some of which are scattered over a surprisingly wide range; e.g. D^0_0(Mg–O). In summary, these ab initio calculations provide a basic set of recommended values, believed to be accurate, and which we use in the interpretation of the experimental flame–ion data. In some cases, experimental flame determinations discussed below will be compared with the calculated and literature values; for some of these, the calculations provide the only source available for comparison. In other cases, the calculated values

Table 4
Recommended standard enthalpies of formation $\Delta H^0_{f,T}$ at 0 K and 298.15 K[a,b]

Species	$\Delta H^0_{f,0}$ at 0 K (kJ mol^{-1}) *(kcal mol^{-1})*	$\Delta H^0_{f,298}$ at 298.15 K (kJ mol^{-1}) *(kcal mol^{-1})*
Mg (^1S)	145.90 ± 0.80	147.10 ± 0.80 [8,15]
	34.9	*35.2*
Mg^+ (^2S)	883.7 ± 1.3	884.8 ± 1.3[c] [8,15]
	211.2	*211.5*[c]
MgO ($^1\Sigma^+$)	149.8	149.4
	35.8	*35.7*
MgOH ($^2\Sigma$)	−105.0	−106.3
	−25.1	*−25.4*
$MgOH^+$ ($^1\Sigma$)	603.3	601.2
	144.2	*143.7*
$MgOH_2^+$ (C_s)	526.8	521.3
	125.9	*124.6*
$Mg(OH)_2$ (C_2)	−524.3	−527.6
	−125.3	*−126.1*
$HOMgOH_2^+$ (C_{2v})	159.4	152.3
	38.1	*36.4*
$MgOH^+ \ldots (OH_2)$[d] (C_s)	257.7	267.4
	65.9	*63.9*

[a] Refer to footnote d of Table 3.
[b] All of the values listed for ions refer to the ion (stationary electron) convention.
[c] Refer to footnote f of Table 3.
[d] Refer to footnote g of Table 1.

Table 5
Thermodynamic quantities derived from the data in Table 4[a,b]

Thermodynamic quantity	Derived values (kJ mol^{-1}) *(kcal mol^{-1})*	Literature values[c] *(kcal mol^{-1})*
$PA^0_{298}(MgO)$	1078.2	*236* [8]; *256 ± 7* [9]; *235 ± 12* [10]
	257.8	
$PA^0_{298}(MgOH)$	902.4	
	215.7	
$PA^0_{298}[Mg(OH)_2]$	850.1	
	203.2	
$IE^0_0(Mg)$	737.8	
	176.3	
	7.647eV	7.646 24 eV [8]; 7.646 eV [35,40]
$IE^0_0(MgOH)$	708.3	
	169.3	
	7.341eV	7.5 ± 0.3 eV [8,10]; 7.3 ± 0.1 eV [9]
$D^0_0(Mg–O)$	242.9	*59 ± 5* [9]; *80 ± 6* [15]; *98 ± 2* [17];
	58.1	*86 ± 2* [41,42]; *64.6 ± 2* [43];[d] *53.5 ± 2* [44];[d] *81 ± 5* [45]; *96 ± 2* [46]
$D^0_0(Mg–OH)$	289.3	*67 ± 6* [9]; *74 ± 5* [10]; *83 ± 5* [15];
	69.1	*76.2 ± 4.1* [16]; *56 ± 5* [17]
$D^0_0(MgO–H)$	470.8	*95 ± 7* [10]
	112.5	
$D^0_0(HOMg–OH)$	457.7	*112 ± 9* [15,42]
	109.4	
$D^0_0(HO–Mg^+)$	318.8	*75 ± 4* [9]; *76 ± 7* [10]; *81.7* [15]
	76.2	
$D^0_0(H_2O–Mg^+) = \Delta H^0_{0,hyd}(Mg^+)$	118.0	*60 ± 5* [9]; *31.2* [47]; *32.8* [48];[d]
	28.2	*25.0* [49]; *38.14* [50][d]
$D^0_0(H_2O–MgOH^+) = \Delta H^0_{0,hyd}(MgOH^+)$	205.0	*57.0* [50];[d] *44* [51]
	49.0	
$\Delta H^0_{298,hyd}(Mg^+)$	121.7	
	29.1	
$\Delta H^0_{298,hyd}(MgOH^+)$	207.1	
	49.5	

[a] Refer to footnote d of Table 3.
[b] Refer to footnote b of Table 4.
[c] Most of the literature values are quoted in *kcal mol^{-1}*; when given in eV, they have been converted using 1 eV = *23.0605 kcal mol^{-1}* where necessary.
[d] These are calculated values, as opposed to experimental.

constitute the basis of the flame experiments. An obvious example would be the percentage composition of the total magnesium present in the flames as neutral Mg, MgO, MgOH, and $Mg(OH)_2$.

3. Experimental

Six premixed, laminar, H_2–O_2–N_2 flames, five of fuel-rich composition (equivalence ratio $\phi = 1.5$) and the other fuel-lean ($\phi = 0.75$), at atmospheric pressure were employed for this work spanning a temperature range 1820–2400 K [14]. Their properties including the calculated composition of the equilibrium burnt gas based on the JANAF Tables [15] are given in Table 6. The concentrations of free radicals overshoot their equilibrium values in the flame reaction zone and then decay downstream toward equilibrium in the burnt gas. The actual concentration is obtained using Sugden's disequilibrium parameter γ [3], defined as the ratio of the local concentration of a radical at a given position in the flame to its final

Table 6
Properties of the hydrogen–oxygen–nitrogen flames

Flame number/ property	2	25	3	4	5	7
$H_2/O_2/N_2$	2.74/1/2.95	3.0/1/3.5	3.18/1/4.07	3.09/1/4.74	3.12/1/5.77	1.5/1/3.55
Total unburnt gas flow ($cm^3\ s^{-1}$)	300	250	250	200	150	250
Equivalence ratio ϕ	1.5	1.5	1.5	1.5	1.5	0.75
Measured flame temperature (K)	2400	2230	2080	1980	1820	2080
Rise velocity in burnt gas ($m\ s^{-1}$)	19.8	18.6	15.6	11.4	8.4	13.2
Equilibrium burnt gas composition (mole fractions)						
H_2O	0.3460	0.3063	0.2754	0.2553	0.2249	0.2802
H_2	0.1286	0.1527	0.1622	0.1390	0.1259	0.000 665 0
O_2	0.000 105 7	0.000 007 90	0.000 000 72	0.000 000 18	0.000 000 01	0.044 39
H	0.006 019	0.002 650	0.001 077	0.000 500 8	0.000 141 5	0.000 068 95
OH	0.003 084	0.000 795 1	0.000 213 0	0.000 088 90	0.000 017 54	0.003 385
O	0.000 094 69	0.000 009 35	0.000 000 99	0.000 000 23	0.000 000 01	0.000 246 2
N_2	0.5157	0.5375	0.5610	0.6052	0.6490	0.6668
Magnesium species (%)						
Mg	32.44	27.37	19.72	12.77	6.65	0.10
MgOH	4.09	2.90	1.91	1.27	0.62	0.15
$Mg(OH)_2$	63.47	69.73	78.37	85.96	92.73	99.75
MgO	0.001 829	0.000 443 9	0.000 102 6	0.000 034 70	0.000 004 632	0.000 128 4

equilibrium value given in Table 6; γ can achieve large values (>100) close to the reaction zone of the cooler flames before decaying downstream towards unity. For fuel-rich flames where H_2O and H_2 are major product species, $\gamma_H = \gamma_{OH} \equiv \gamma$ and $\gamma_O = \gamma^2$; for fuel-lean flames, the γ dependence is different. Plots of γ versus axial distance z are available for the five fuel-rich flames listed in Table 6 [14]; thus, the radical concentrations are known at all points in the flames. These pseudo-one-dimensional flat flames in plug flow were stabilized on a water-cooled brass burner [52], and were cylindrical in shape with a diameter of about 12 mm.

Magnesium was introduced into the flames by spraying an aqueous solution of either the acetate $MgAc_2.4H_2O$ (BDH, >98% pure) or the chloride $MgCl_2.6H_2O$ (Caledon Laboratories, >99% pure) as an aerosol from an atomizer [53] into the nitrogen supply of the premixed flame gas. Spraying a 0.1 M solution introduced 9.5×10^{-7} mole fraction of total magnesium into the premixed flame gas. To ascertain the difference between the acetate and the chloride, a zinc acetate $ZnAc_2$ (Aldrich, 99.99% pure) solution and also a $ZnCl_2$ (BDH, >97%) solution were sprayed because zinc does not produce any metallic flame ions [54]. All of these salt samples contained very small amounts of potassium present as an impurity which produced K^+ ions by collisional (thermal) ionization in the flames. The K^+ signals were not related to the stated purity of the salt; e.g. the impurity signal was smallest for the $MgAc_2.4H_2O$. The presence of magnesium did not impart any noticeable colour to the flames. These flames exhibit only a low level of natural ionization. For ion recombination studies, it was advantageous to add 0.25 mol% of CH_4 to the premixed flame gas to produce a high initial concentration of H_3O^+ stemming from the chemi-ionization reaction of CH + O near the flame reaction zone; these ions subsequently decay downstream by electron–ion recombination. With the simultaneous addition of magnesium, H_3O^+ produced magnesium ions by chemical ionization (CI) processes. The addition of CH_4 was small enough so that the flame composition and temperature remained essentially unchanged.

The burner is mounted horizontally on a motorized carriage with calibrated drive coupled to the *X* axis of an *XY* recorder. The flame axis *z* is accurately aligned with the sampling nozzle of the mass spectrometer. The apparatus has been described in detail previously

[52] so only a brief description will be given here. Flame gas containing ions is sampled through an orifice in the tip of a conical nozzle protruding from a water-cooled sampling plate. A series of blunt nozzles employing electron microscope lenses of Pt/Ir alloy had diameters in the range 0.078–0.202 mm. A sharper, 60°, electroformed, nickel nozzle of orifice diameter 0.198 mm exhibited less cooling in the boundary layer and was used when it was desired to minimize the formation of ion hydrates. The ions enter a first vacuum chamber maintained at 0.04 Pa (3×10^{-4} Torr), and are focused into a beam by an electrostatic lens. The beam then passes through a 3 mm orifice into a second vacuum chamber maintained below 0.003 Pa (2×10^{-5} Torr). The ions traverse a second ion lens into a quadrupole mass filter. They are detected by a Faraday collector connected to a vibrating reed electrometer having a grid-leak resistor of 10^{10} Ω; the ion signal is applied to the *Y* axis of the *XY* recorder. The signal magnitudes quoted in the following figures as a voltage (in mV) refer to the collected ion current passing through 10^{10} Ω. By driving the flame towards the sampling nozzle, profiles were obtained of an individual ion versus distance along the flame axis *z*.

As an alternative to individual ions, total positive ion (TPI) profiles can be measured by switching off the dc voltages to the quadrupole rods. However, the sensitivity of the mass spectrometer is different for individual ions and TPI because the former are measured at fairly high resolution whereas total ion collection amounts to zero resolution. The former sensitivity is approximately one half of the latter. The zero on the *X* axis ($z = 0$) was defined experimentally where the pressure abruptly rises when the sampling nozzle pokes through the flame reaction zone into the cooler unburnt gas upstream. The pressure is measured with an ionization gauge mounted on the wall of the second vacuum chamber. Negative magnesium ions were not detected in the fuel-rich flames. Since a flame is a quasineutral plasma, [TPI] is equal to [e^-], the concentration of free electrons. Calibration procedures for the atomizer delivery into the flame gas and for the mass spectrometer sensitivity have been given previously [55,56]. When the gas is sampled through the nozzle, it cools in two regions: in the thermal boundary layer surrounding the orifice and in the near-adiabatic expansion downstream of the nozzle throat. This can cause a shift of fast equilibrium reactions in the exothermic direction during sampling. In particular, the signals of ion hydrates which may not be genuine flame ions can be enhanced with respect to that of the parent ion. These sampling problems have been discussed in considerable detail [57–59]. Of course, when [TPI] is measured, the hydrate ions are included along with the parent ions.

4. Results and discussion

4.1. Neutral magnesium species in flames

Magnesium can be present in these flames as the four neutral species Mg, MgOH, $Mg(OH)_2$, and MgO. Because of the relatively weak Mg–OH bond, the monohydroxide might be formed either by a fast, balanced, two-body process (denoted by an equals to sign)

$$Mg + H_2O = MgOH + H \quad (1)$$

or by a three-body process which is not necessarily balanced (denoted by a double arrow ⇄)

$$Mg + OH + M \rightleftarrows MgOH + M \quad (2)$$

Additional fast balanced reactions produce the dihydroxide and the oxide [2,7]

$$MgOH + H_2O = Mg(OH)_2 + H \quad (3)$$

$$Mg + H_2O = MgO + H_2 \quad (4)$$

That reaction (3) proceeds via the two-body process is not in doubt according to the Sugden criterion [11] because the second hydroxyl bond is strong, i.e. D_0^0(HOMg–OH) = 457.7 kJ mol^{-1} from Table 5. The relative equilibrium concentrations of the four magnesium neutral species have been calculated using data from the JANAF Tables [15] and are given in Table 6 for all six flames; the magnesium ions constitute only a negligible fraction of the total magne-

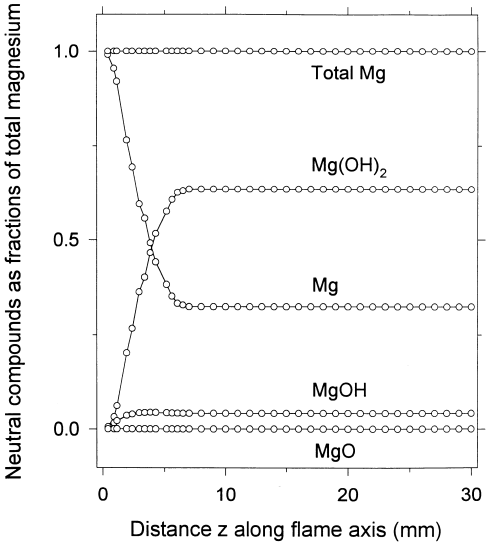

Fig. 2. Profiles of magnesium neutral compounds along the axis z of flame 2 at 2400 K. The reaction zone is located upstream of $z = 0$.

sium present. Because reactions (1)–(3) involve the radicals H and OH, the relative concentrations depend on the disequilibrium parameter γ and vary downstream wherever γ varies; equations for the γ dependence have been given by Hayhurst and Kittelson [4].

Calculated neutral profiles of the four magnesium species along the axis of flame 2 are given in Fig. 2. It has been assumed that all of the magnesium is initially present upstream as atomic Mg after dissociation of the acetate or chloride salt in the reaction zone. For this flame at a temperature of 2400 K, all four neutrals exhibit constant equilibrium values for $z > 7$ mm where $\gamma = 1$ [14]. By contrast, in a similar plot for flame 3 (not shown), γ decreases throughout the whole 30 mm of flame and has not reached unity even at $z =$ 30 mm downstream [14]. Consequently, the relative neutral concentrations do not quite achieve their constant equilibrium values given in Table 6. It is evident that magnesium is different from the other alkaline earth metals Ca, Sr, and Ba in fuel-rich flames; although $[Mg(OH)_2]$ is the dominant species, atomic [Mg] > [MgOH]. This will not necessarily be the case in fuel-lean flames, however. In all of the flames in Table 6, MgO is a minor species with [MgO] < 0.002%. It is also worth mentioning that no visual evidence was obtained for the formation of solid particles when magnesium was added to these flames.

4.2. Ionic species and profiles

Magnesium has three stable isotopes: ^{24}Mg (78.99%), ^{25}Mg (10.00%), and ^{26}Mg (11.01%) [60]. A mass spectrum measured at high resolution is given in Fig. 3 for flame 3 with the atomizer spraying a 0.1 M solution of $MgAc_2.4H_2O$ showing all of the ions observed downstream at $z = 30$ mm. As expected [6], Mg^+ shows the largest signal with smaller amounts of its first and second hydrates. It is probable that most of the hydrate signals arise due to cooling during sampling except that the magnitude of $Mg^+.H_2O$ ($=MgOH_2^+$) is larger than expected when using a Pt/Ir sampling nozzle of diameter 0.170 mm; this argues in favour of a contribution from protonation of the abundant neutral MgOH. Impurity signals due to Na^+ at 23 u and K^+ at 39 u are evident with only a small isotopic contribution at 41 u (potassium is 93.258% ^{39}K, 0.012% ^{40}K, 6.730% ^{41}K). Thus, most of the very small signal at 41 u comes from $MgOH^+$ interpreted as protonated MgO; the small magnitude reflects the low abundance of neutral MgO. However, its first, second and even third hydrate ion signals are larger. Presumably protonation of the abundant neutral $Mg(OH)_2$ is involved in addition to hydrate enhancement by sampling cooling.

Fig. 4 shows ion profiles measured with the mass spectrometer at high resolution using a sharp Ni nozzle of orifice diameter 0.198 mm with the atomizer spraying a 0.05 M solution of $MgAc_2.4H_2O$ into the second coolest fuel-rich flame 4. The ions are dominated by atomic Mg^+. High resolution was necessary to separate the very small $MgOH^+$ signal at 41 u from that of $Mg^+.H_2O$ ($=MgOH_2^+$) at 42 u; the latter hydrate signal is undoubtedly enhanced by sampling cooling. These profile shapes are fairly typical of those observed in all five fuel-rich flames in that Mg^+ and its hydrate rise to plateau values whereas the $MgOH^+$ signal decays downstream. By way of contrast, Fig. 5 gives profiles using a blunt Pt/Ir nozzle of orifice diameter 0.170 mm with the atomizer spraying a 0.1 M solution of $MgAc_2.4H_2O$ into the fuel-lean

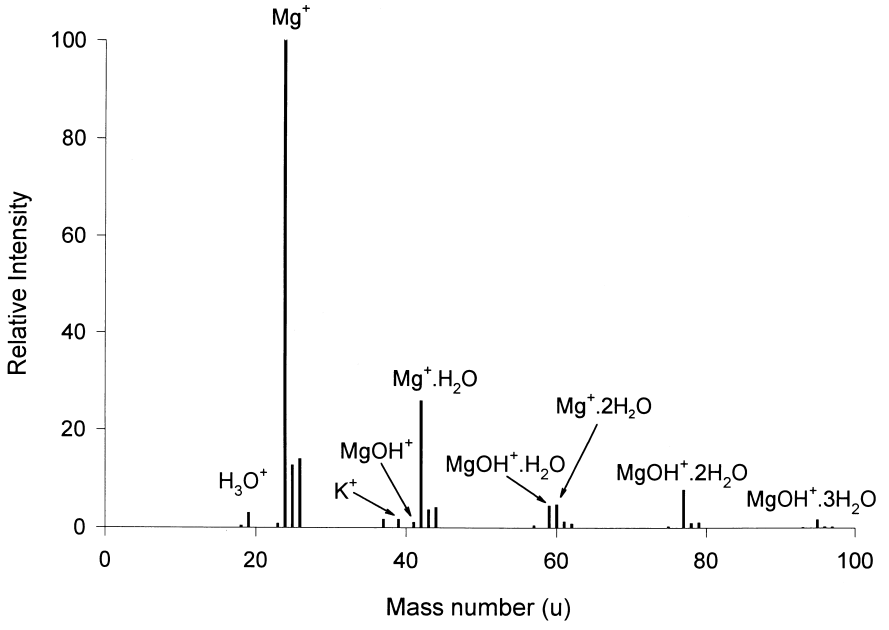

Fig. 3. Mass spectrum at high resolution measured downstream at $z = 30$ mm in flame 3 with the atomizer spraying a 0.1 M $MgAc_2$ solution when a 0.170 mm Pt–Ir sampling orifice was used.

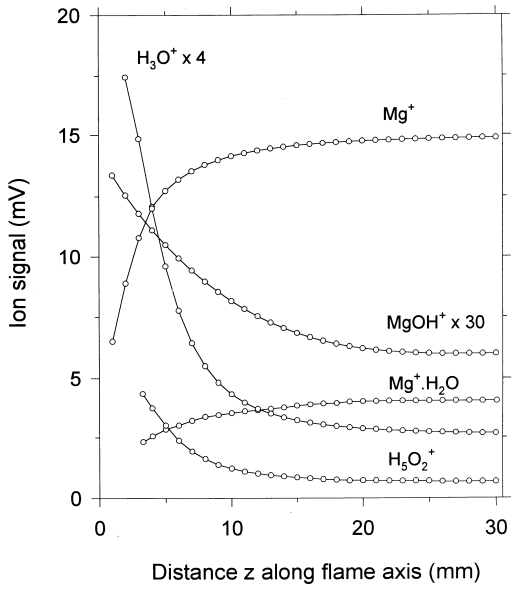

Fig. 4. Ion profiles measured in flame 4 vs. axial distance z, with the atomizer spraying a 0.05 M $MgAc_2$ solution when a 0.198 mm Ni sampling orifice was used. The reaction zone is located upstream of $z = 0$.

flame 7. The observed ions can be organized into the same two hydrate series $Mg^+.nH_2O$ ($n = 0, 1$) and $MgOH^+.nH_2O$ ($n = 1, 2, 3$; the parent ion with $n = 0$ was too small to be observed). However, the profile shapes are different in that Mg^+ ions now decay and $MgOH^+$ ions rise downstream. An understanding of the ion chemistry must lead to an explanation of these patterns of behaviour.

4.3. Ionic reactions and the interconversion of $Mg^+/MgOH^+$

It is helpful at this stage to formulate a fairly complete list of reactions which may be involved in the production and loss of magnesium ions. In the absence of magnesium, the natural H_3O^+ flame ion is produced by the chemi-ionization reaction [61,62]

$$H + H + OH \rightleftarrows H_3O^+ + e^- \quad (5)$$

With added metal, the magnesium ions can be formed by CI of neutral magnesium species via proton transfer from H_3O^+

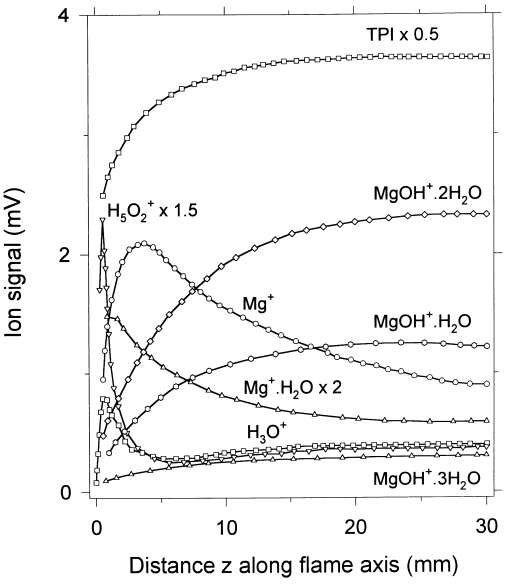

Fig. 5. Ion profiles measured in flame 7 vs. axial distance z, with the atomizer spraying a 0.1 M $MgAc_2$ solution when a 0.170 mm Ni sample orifice was used. TPI denotes total positive ions. The reaction zone is located upstream of $z = 0$.

$$H_3O^+ + MgO \rightleftarrows H_2O + MgOH^+ \quad (6)$$

$$H_3O^+ + MgOH \rightleftarrows H_2O + MgOH_2^+ \text{ or } Mg^+.H_2O \quad (7)$$

$$H_3O^+ + Mg(OH)_2 \rightleftarrows H_2O + HOMgOH_2^+ \text{ or } MgOH^+.H_2O \quad (8)$$

Proton transfer can also occur amongst ionic and neutral magnesium species. Because $[H_2O]$ is large, it can be assumed that hydration reactions of magnesium ions are rapid and balanced, e.g.

$$Mg^+ + H_2O + M = MgOH_2^+ + M \quad (9)$$

$$MgOH^+ + H_2O + M = HOMgOH_2^+ + M \quad (10)$$

The Mg^+ and $MgOH^+$ ion series may be linked either by a two-body or a three-body process

$$Mg^+ + H_2O \rightleftarrows MgOH^+ + H \quad (11)$$

$$Mg^+ + OH + M \rightleftarrows MgOH^+ + M \quad (12)$$

similar to the neutral reactions (1) and (2); the operative reactions will depend on the HO–Mg^+ bond strength with reference to the Sugden criterion [11]. In common with Ca, Sr, and Ba, $MgOH^+$ might also be produced by the chemi-ionization reactions

$$Mg + OH \rightleftarrows MgOH^+ + e^- \quad (13)$$

$$MgO + H \rightleftarrows MgOH^+ + e^- \quad (14)$$

As to ion loss mechanisms, the major atomic Mg^+ ion will recombine by a slow three-body process

$$Mg^+ + e^- + M \rightarrow Mg + M \quad (15)$$

The reverse reaction (−15) which amounts to collisional (thermal) ionization is not included; it would be very slow due to the high ionization energy, $IE^0(Mg) = 176.3$ kJ mol^{-1} [8,35,40]. All of the molecular magnesium ions $MgH_mO_n^+$ can undergo relatively fast dissociative recombination by two-body processes

$$MgH_mO_n^+ + e^- \rightarrow \text{neutral products} \quad (16)$$

with recombination coefficients $k_{15} \approx 10^{-7}$ cm^3 molecule^{-1} s^{-1}; examples would be reactions (−13) and (−14), or possibly multiple channels if hydrates are involved, e.g.

$$MgOH_2^+ + e^- \rightarrow Mg + H_2O \text{ or } MgOH + H \quad (17)$$

A method is available to distinguish reactions (11) and (12). Where K is the equilibrium constant, $[MgOH^+]/[Mg^+] = (K_{11}[H_2O]/[H]_{eq})(1/\gamma) = (K_{12}[OH]_{eq}[M]/[M])\gamma$; i.e. the ion ratio is proportional to $1/\gamma$ for reaction (11), but is proportional to γ for reaction (12). Fig. 6 gives plots of $[MgOH^+]/[Mg^+]$ versus γ [Fig. 6(a)] and versus $1/\gamma$ [Fig. 6(b)] from profiles measured at high resolution in flame 25 for the range $z = 2$–10 mm where γ undergoes a large change [14]; the atomizer was spraying a 0.1 M solution of $MgAc_2.4H_2O$. It is fairly clear that the plot versus γ yields a straight line, unlike the inverse γ plot, such that reaction (12) appears to be operative. A similar, although unpublished, conclusion was reached by Hayhurst [63]. This experimental finding is essentially in line with Sugden's criterion for D_0^0(HO–Mg^+) ≈ 335 kJ mol^{-1} [11] whether the value of 314 ± 17 [9], 318 ± 29 [10] (similar to our derived

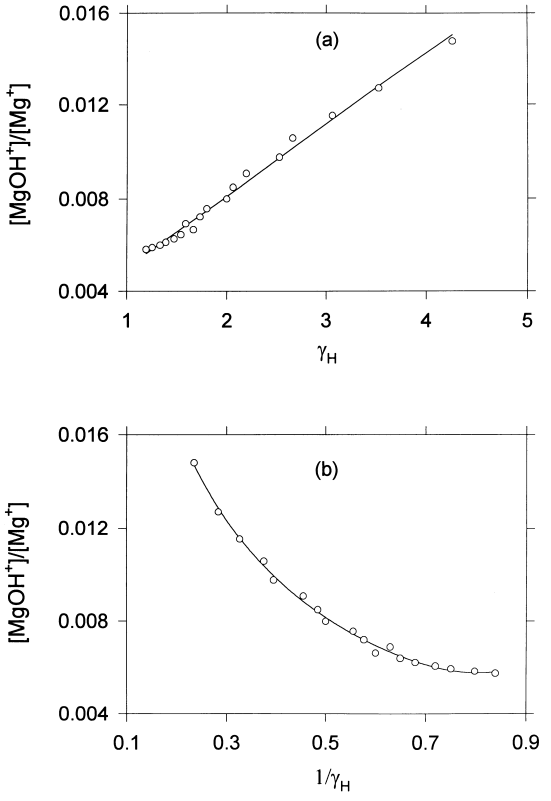

Fig. 6. Plots of $[MgOH^+]/[Mg^+]$ vs. (a) γ and (b) $1/\gamma$ in flame 25, with the atomizer spraying a 0.1 M solution of $MgAc_2$.

value of 318.8), or 342 kJ mol^{-1} [15] is considered. Although it is possible that both reactions play a role, reaction (12) will be invoked henceforth. A plot of ln K_{12} versus 1/T gives a very good straight line; a least squares fit yields $K_{12} = 7.430 \times 10^{-6}$ exp(38240/T) for the flame temperature range 1820–2400 K, or 5.903×10^{-6} exp(38 680/T) for the whole temperature range 298–2500 K. The exponent D^0/RT amounts very closely to the endothermicity of reaction (12) which, at 0 K, is $D_0^0(HO–Mg^+) = 318.8$ kJ mol^{-1}. Potentially, reaction (12) for a metal ion $HO–A^+$ with a weak bond is of considerable significance for flame studies if the reaction is (1) rapidly equilibrated, (2) dominant over reaction (11) and (3) unaffected by sampling errors, i.e. the equilibrium does not shift because of a change in sample cooling when the diameter of the sampling orifice is varied. If K_{12} is known, then [OH] can be determined from the measurement of the $[AOH^+]/[A^+]$ ion ratio. Since [OH] at equilibrium can be calculated, values of γ are obtained at any point on the flame axis. In the present case of magnesium in fuel-rich flames, the $MgOH^+$ signals are too small to provide reliable quantitative data. The point is of particular significance for fuel-lean flames where OH is the major radical species and other possible methods for the measurement of radical concentrations (i.e. γ) are uncertain. However, the investigation of a range of fuel-lean flames was beyond the scope of the present study, but should be pursued in the future.

4.4. Proton affinity of MgO

In Fig. 4 the $MgOH^+$ and H_3O^+ profiles fall downstream of the flame reaction zone and achieve constant plateau values indicative of chemical equilibrium towards $z = 30$ mm. By adjusting the concentration of the magnesium solution in the atomizer, it was possible to achieve these plateau values of the two ion profiles in all five fuel-rich flames. The two ions relate to reaction (6) for proton transfer between MgO and H_2O whose reaction enthalpy $\Delta H^0(6) = PA^0(H_2O) - PA^0(MgO)$, the difference of their proton affinities. The equilibration of reaction (6) requires that the relaxation time $\tau_6 = 1/(k_6[MgO] + k_{-6}[H_2O])$ be appreciably less than the time corresponding to 30 mm of flame represented by $\Delta z/v$; v is the (average) rise velocity of approximately 15 m s^{-1} corresponding to 2 ms (milliseconds). A straightforward calculation of τ_6 yields a value of the order of 10 ms which is too large; it occurs because [MgO] is a minor constituent, as shown in Table 6. The answer lies in the fact that there is another route to form $MgOH^+$ involving proton transfer by H_3O^+ to the major constituent $Mg(OH)_2$ via reaction (8) followed by rapid dissociation of the $HOMgOH_2^+$ ion to give $MgOH^+$ via reaction (−10). The inclusion of $[Mg(OH)_2]$ from Table 6 into the expression for τ_6 yields a value of the order of 0.1 ms such that the assumption of equilibrium is warranted. It is also important that τ_6 is greater than the sampling time of 1 μs so that the equilibrium ion ratio does not shift due to cooling during sampling. In summary, the

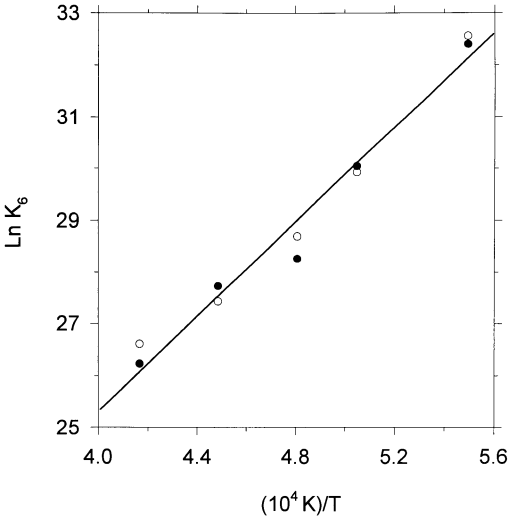

Fig. 7. Van't Hoff plot for the equilibrium constant of the proton transfer reaction (6) involving $MgOH^+$ and H_3O^+ measured in five flames over the temperature range 1820–2400 K. The solid circles refer to a 0.1 M $MgAc_2$ solution sprayed by the atomizer using a Pt–Ir (flat) nozzle of orifice diameter 0.170 mm, and the open circles to a 0.05 M solution with a Ni (sharp) nozzle of diameter 0.198 mm.

kinetic considerations and flame conditions are correct for equilibrium to be attained.

Fig. 7 presents a van't Hoff plot of ln K_6 versus $1/T$ for the five fuel-rich flames covering the temperature range 1820–2400 K, where $K_6 = ([MgOH^+]/[H_3O^+])([H_2O]/[MgO])$. Because the $MgOH^+$ signals were so small, it was more accurate to measure $[Mg^+]$ and obtain $[MgOH^+]$ from K_{12} derived in the previous section. The ion ratios were measured downstream near $z = 30$ mm; the neutral ratios were calculated from the data in Table 6 and appropriate values of γ. If the ion ratios were multiplied by a constant factor representative of mass discrimination, the slope of the van't Hoff plot would not change although the intercept would be affected. The same would be true if the ion ratios were modified by a constant hydrate contribution. This important consideration lends credibility to thermodynamic values derived from the slope. Two sets of data are given in Fig. 7: the solid circles were obtained with the atomizer spraying a 0.1 M solution of $MgAc_2.4H_2O$ using a blunt Pt/Ir nozzle of orifice diameter 0.170 mm, and the open circles with a 0.05 M solution and a sharp Ni nozzle of diameter 0.198 mm. The slope of the least-squares fit of a good straight line to the data yields $\Delta H^0_{2100}(6) = -376.9 \pm 22.9$ kJ mol^{-1} (standard deviation) centred on the average flame temperature of 2100 ± 50 K, or $\Delta H^0_{298}(6) = -364.8 \pm 22.9$ kJ mol^{-1} corrected to 298.15 K. With the currently accepted value of $PA^0_{298}(H_2O) = 691.0$ kJ mol^{-1} [8], $PA^0_{298}(MgO)$ is 1056 kJ mol^{-1} *(252.3 kcal mol^{-1})*, in reasonable agreement with our derived (calculated) value of 1078.2 kJ mol^{-1} *(257.8 kcal mol^{-1})* corrected to 298.15 K. When experimental errors are included, our data yield $PA^0_{298}(MgO) = 1056 \pm 29$ kJ mol^{-1} *(252 ± 7 kcal mol^{-1});* however, it is based on the calculated thermodynamic data in Table 4 for Mg, MgO, MgOH, and $Mg(OH)_2$.

4.5. Proton affinities of MgOH and $Mg(OH)_2$

The hydration of Mg^+ in the balanced reaction (9) yields $Mg^+.H_2O$ or $MgOH_2^+$ which is assumed to be protonated MgOH. The hydration enthalpy of Mg^+ is $\Delta H^0_{hyd}(Mg^+) = -\Delta H^0_9$, and the proton affinity is given by $PA^0(MgOH) = \Delta H^0_{hyd}(Mg^+) - IE^0(Mg) + IE^0(H) - D^0(Mg–OH) + D^0(H–OH)$. All of these quantities are known except $\Delta H^0_{hyd}(Mg^+)$ which can be determined from measurements of the ion ratio $[MgOH_2^+]/[Mg^+]$. However, reaction (9) is sufficiently fast that it shifts to the right in the exothermic direction due to cooling during sampling. Presumably most of this cooling occurs when the ions pass though the cold boundary layer surrounding the orifice in the tip of the sampling nozzle. As the orifice becomes progressively larger, the influence of the boundary layer is reduced and the ion ratio decreases; the true ion ratio effectively corresponds to an orifice of infinite diameter d. This may be found by measuring the ion ratio at $z = 30$ mm downstream for a series of orifices of different sizes, plotting the ratio versus inverse area (i.e. $\propto 1/d^2$) and extrapolating to zero. A similar method has been employed many times by Hayhurst and his co-worker, and is discussed in considerable detail in a recent publication [14]. The method has been applied in Fig. 8 to flame 3 at 2080 K (open circles) and flame 2 at 2400 K (solid circles)

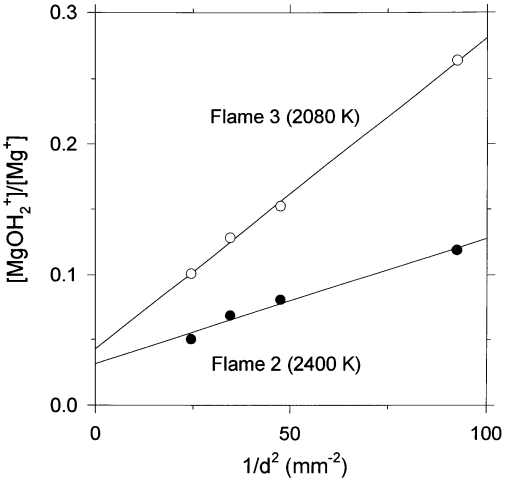

Fig. 8. Plots of $[MgOH_2^+]/[Mg^+]$ vs. $1/d^2$ measured downstream at $z = 30$ mm in flames 2 and 3, where d is the diameter of the sampling orifice.

using four blunt Pt/Ir nozzles with orifice diameters 0.104, 0.145, 0.170, and 0.202 mm. Straight lines through the points fitted by least squares give extrapolated values for the ion ratio $[MgOH_2^+]/[Mg^+]$ of 0.042 78 (flame 3) and 0.031 37 (flame 2) from which K_9, and thus ΔG_9^0, may be determined. The sampled gas achieves a speed of Mach 1 at the orifice throat (the narrowest part) and the assumption is made that the chemistry is frozen downstream of this point. Thus, the extrapolated ion ratios correspond to the throat temperatures T_t and not the flame temperatures T_f. The two are related by the expression $T_t = 2T_f/(1 + \gamma^*)$ [14], where in this case $\gamma^* = C_p/C_v$, the ratio of the specific heats (not the disequilibrium parameter). For flame 3, $\gamma^* = 1.2612$, $T_t = 1840$ K, $[H_2O] = 0.2758$, $K_9 = 0.1551$, and $\Delta G_9^0 = 28.51$ kJ mol^{-1}; for flame 2, $\gamma^* = 1.2446$, $T_t = 2138$ K, $[H_2O] = 0.3506$, $K_9 = 0.089\,48$ and $\Delta G_9^0 = 42.91$ kJ mol^{-1}. The equilibrium values of $[H_2O]$ expressed as mol fractions have been recalculated at the lower throat temperatures.

To find $\Delta H_9^0 = \Delta G_9^0 + T\Delta S_9^0$, it was necessary to evaluate ΔS_9^0 from absolute entropy values which are provided by the JANAF Tables [15] for H_2O and Mg^+ (which agrees with our calculations) but not for $Mg^+.H_2O$ (or $MgOH_2^+$). A statistical calculation of $S_T^0(MgOH_2^+)$ was carried out using rotational and vibrational temperatures given in Table 2. For flame 3, the calculated values are $S_{1840}^0(MgOH_2^+) = 366.8$ J mol^{-1} K^{-1} with $\Delta S_{1840}^0 = -85.9$ J mol^{-1} K^{-1}, and $\Delta H_{1840}^0 = -129.6$ kJ mol^{-1} for the reaction. For flame 2, the values are $S_{2138}^0(MgOH_2^+) = 378.0$ J mol^{-1} K^{-1} with $\Delta S_{2138}^0 = -85.6$ J mol^{-1} K^{-1} and $\Delta H_{2138}^0 = -140.0$ kJ mol^{-1}. To correct the ΔH_T^0 values to 298.15 K, the enthalpy function $H_T^0 - H_{298}^0 = (H_T^0 - H_0^0) - (H_{298}^0 - H_0^0)$ was calculated by statistical methods for $MgOH_2^+$ and obtained from the JANAF Tables [15] for Mg^+ and H_2O giving $\Delta H_{298}^0 = -132.8$ for flame 3 and -144.0 kJ mol^{-1} for flame 2; the average value is -138.4 kJ mol^{-1}, i.e. $\Delta H_{hyd}^0(Mg^+) = 138.4$ kJ mol^{-1} at 298.15 K. The experimental method with its empirical extrapolation technique is crude so that a large error limit of ± 29 kJ mol^{-1} *(± 7 kcal mol^{-1})* is warranted. Corrected to 0 K, $\Delta H_{hyd}^0(Mg^+)$ amounts to a bond dissociation energy $D_0^0(H_2O–Mg^+) = 134.5$ kJ mol^{-1} (or *32.15 kcal mol^{-1}* = 1.394 eV). The results of the ab initio calculation give $\Delta H_{hyd}^0(Mg^+) = 121.7$ kJ mol^{-1} at 298.15 K.

For the evaluation of the proton affinity, values at 298.15 K for $IE^0(Mg)$, $IE^0(H)$, and $D^0(H–OH)$ were taken from the JANAF Tables [15] giving $PA_{298}^0(MgOH) = 919.1$ kJ mol^{-1} *(219.7 kcal mol^{-1})* with $D^0(Mg–OH) = 292.4$ kJ mol^{-1} based on Table 4. This is in reasonable agreement with the derived value of 902.4 kJ mol^{-1} given in Table 5 from the ab initio calculations.

In exactly the same way, the hydration of $MgOH^+$ in the balanced reaction (10) yields $MgOH^+.H_2O$ or $HOMgOH_2^+$ which is assumed to be the same ion as $Mg(OH)_2.H^+$, i.e. protonated $Mg(OH)_2$. The hydration enthalpy of $MgOH^+$ is $\Delta H_{hyd}^0(MgOH^+) = -\Delta H_{10}^0$, and the proton affinity is given by $PA^0[Mg(OH)_2] = \Delta H_{hyd}^0(MgOH^+) - IE^0(MgOH) + IE^0(H) - D^0(HOMg–OH) + D^0(H–OH)$. All of these quantities are known except $\Delta H_{hyd}^0(MgOH^+)$, which can be determined from measurements of the ion ratio $[HOMgOH_2^+]/[MgOH^+]$. The experimental ion ratios are plotted in Fig. 9 versus $1/d^2$ and give extrapolated intercept values corresponding to infinite orifice diameter of 1.371 for flame 3 and 1.025 for flame 2

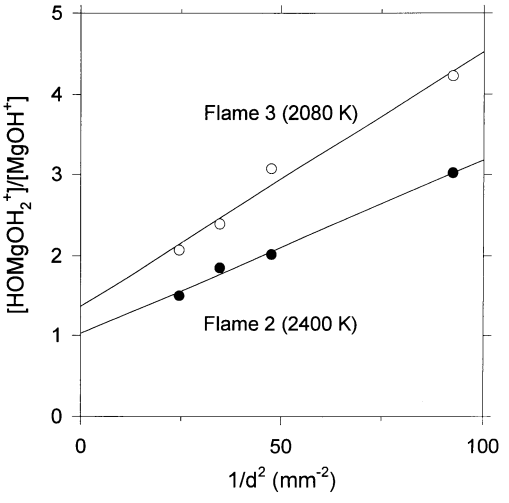

Fig. 9. Plots of $[HOMgOH_2^+]/[MgOH^+]$ vs. $1/d^2$ measured downstream at $z = 30$ mm in flames 2 and 3, where d is the diameter of the sampling orifice.

corresponding to throat temperatures of 1840 and 2138 K, respectively, as before. These yield equilibrium constants $K_{10} = 4.971$ with $\Delta G^0_{10} = -24.53$ kJ mol^{-1} for flame 3, and $K_{10} = 2.924$ with $\Delta G^0_{10} = -19.07$ kJ mol^{-1} for flame 2. Statistical mechanical methods were applied to $HOMgOH_2^+$ and $MgOH^+$ using the rotational and vibrational temperatures given in Table 2; in the latter case, the vibrational frequencies are significantly different from those given in the JANAF Tables [15]. For flame 3, $S^0_{1840}(HOMgOH_2^+) = 493.7$ and $S^0_{1840}(MgOH^+) = 332.9$ J mol^{-1} K^{-1} giving $\Delta S^0_{1840} = -99.8$ J mol^{-1} K^{-1} and $\Delta H^0_{1840} = -208.1$ kJ mol^{-1} for reaction (10). For flame 2, the values are $S^0_{2138}(HOMgOH_2^+) = 511.7$, $S^0_{2138}(MgOH^+) = 341.6$ with $\Delta S^0_{2138} = -98.1$ J mol^{-1} K^{-1} and $\Delta H^0_{2138} = -228.9$ kJ mol^{-1}. Corrected to room temperature, the two flames yield $\Delta H^0_{298} = -223.1$ and -247.1, respectively, for an average value of -235.1 kJ mol^{-1}; i.e. $\Delta H^0_{hyd}(MgOH^+) = 235.1$ kJ mol^{-1}. A similar large error limit of ± 29 kJ mol^{-1} *(±7 kcal mol^{-1})* is appropriate, as was quoted for Mg^+ hydration. The value compares with an hydration enthalpy of 207.1 kJ mol^{-1} from the standard heats of formation at 298.15 K generated by the ab initio calculations for $HOMgOH_2^+$ and $MgOH^+$.

Both the experimental and the theoretical values are surprisingly high but they reinforce each other; they amount to a bond dissociation energy $D^0_0(H_2O–MgOH^+)$ of 230.6 or 205.0 kJ mol^{-1}, respectively. However, this rather strong bond energy offers some explanation for a curious feature of the mass spectrum shown in Fig. 3 where it was observed that the signal magnitude of $HOMgOH_2^+$ ($=MgOH^+.H_2O$ at 59 u) was greater than that of the parent ion $MgOH^+$ (41 u); in fact, that of $MgOH^+.2H_2O$ (77 u) was still larger, although the $MgOH^+.3H_2O$ (95 u) signal was smaller. Normally, the parent ion signal is much greater than those of the hydrates which progressively decrease with increasing hydration number; such hydrates are not genuine flame ions but are formed during sampling cooling. Apparently, this is not the case for magnesium where $Mg(OH)_2$ is a major neutral species with $D^0_0(HOMg–OH) = 457.7$ kJ mol^{-1} from the ab initio calculations. Protonation of one of its OH groups to form $HOMg–OH_2^+$, in this case a genuine flame ion, substantially reduces the Mg–O bond energy down to 205.0 kJ mol^{-1}. The experimental value for $\Delta H^0_{hyd}(MgOH^+) = 235.1$ kJ mol^{-1} yields $PA^0_{298}[Mg(OH)_2] = 878.2$ kJ mol^{-1} *(209.9 kcal mol^{-1})* based on $IE^0_0(MgOH) = 7.341$ eV from Table 5. The ab initio calculations give a value of 850.1 kJ mol^{-1} *(203.2 kcal mol^{-1})*, in reasonable agreement with the flame experiment.

4.6. Recombination of magnesium ions with electrons

In general, slow three-body recombination of the atomic ion Mg^+ by reaction (15) can be ignored in comparison with relatively fast dissociative recombination of molecular ions $MgH_mO_n^+$ by reaction (16) because the pseudo-second-order rate coefficient $k_{15}[M] \ll k_{16}$. Because $[Mg^+]$ is so dominant in the present case as shown in Fig. 3, both reactions might be expected to contribute with comparable rates. In this event, all that can be determined is a global recombination coefficient k_{rec} which encompasses the effects of both processes. Accordingly, a 0.1 M solution of $MgAc_2.4H_2O$ was sprayed with the atomizer into the five fuel-rich flames which were also doped with 0.25 mol% of CH_4 to produce a high

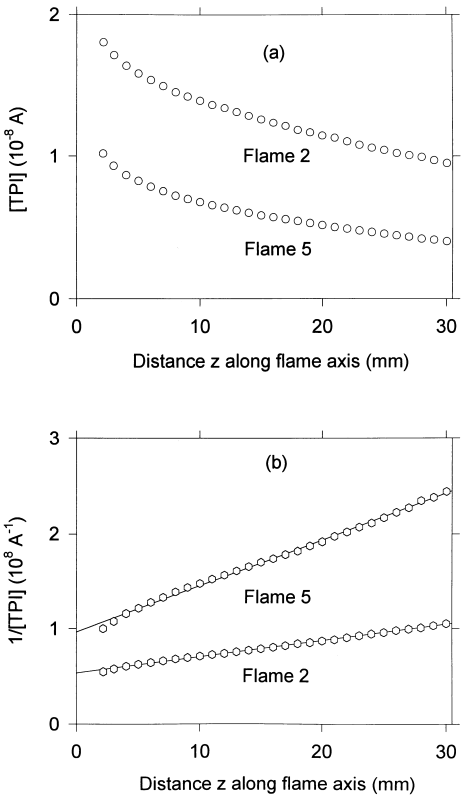

Fig. 10. Electron–ion recombination exemplified by (a) profiles of the total positive ion current [TPI] vs. axial distance z measured in flames 2 and 5 doped with 0.25 mol % of methane and with the atomizer spraying a 0.1 M solution of $MgAc_2$. The profiles are analysed in (b) by inverse plots of 1/[TPI] vs. z whose slope yields the global recombination coefficient.

superequilibrium level of H_3O^+ near the flame reaction zone. The magnesium ions were rapidly formed by the CI reactions (6)–(8) with subsequent hydration and link reactions (9), (10), and (12). Profiles of the total positive ions (TPIs) versus axial distance z were recorded, as shown in Fig. 10(a) for flames 2 and 5. For these experiments, TPI was measured with a sensitive picoammeter connected to the electrostatic ion lens in the first vacuum chamber supplied with an appropriate bias voltage; this technique avoids possible mass discrimination due to tuning effects since tuning of the ion lenses is obviated. Plots of 1/[TPI] versus z gave good straight lines as shown in Fig. 10(b) whose slopes yielded the values of k_{rec}.

Values of the experimental global k_{rec} are given in Table 7, lines (a) and (b), for two runs using five flames on different days with independent calibrations of the absolute ion concentrations in terms of measured ion currents. The two runs are in reasonable agreement but the values of k_{rec} are, seemingly, erratic in that they do not show any uniform trend with decreasing temperature. Thus, an attempt was made to model the overall recombination in terms of reactions (15) and (16); i.e. the rate $= k_{rec}[TPI][e^-] = k_{15}[M][Mg^+][e^-] + k_{16}[MgH_mO_n^+][e^-]$ where $[TPI] = [Mg^+] + [MgH_mO_n^+]$, so that a calculated value of $k_{rec} = k_{15}[M][Mg^+]/[TPI] + k_{16}[MgH_mO_n^+]/[TPI]$. For this model, a value of $k_{15} = 4 \times 10^{-24}$ T^{-1} cm^6 $molecule^{-2}$ s^{-1} was assumed; it is typical for all of the atomic alkali metal ions from Li^+ to Cs^+ [64]; its values at the five flame temperatures are given below line (c) in Table 7. A constant value of $k_{16} = 2 \times 10^{-7}$ cm^3 $molecule^{-1}$ s^{-1} was assumed because it is typical for a wide variety of cations at flame temperatures. The factor $[Mg^+]/[TPI]$ was obtained by recording mass spectra like Fig. 3 well downstream in each flame and measuring the peak heights; clearly, $[MgH_mO_n^+]/[TPI] = 1 - [Mg^+]/[TPI]$. The $\%[Mg^+]$ ions determined in this way are shown for each flame below line (c) in Table 7.

Using these data, the calculated values of k_{rec} are given in line (c). The agreement with lines (a) and (b) is not very good. The calculated values show a steadily increasing trend with decreasing temperature, and the values are too large; evidently $[Mg^+]$ has been underemphasized. Now, suppose that $MgOH_2^+ = Mg^+.H_2O$ (the second largest peak height in Fig. 3) is not a genuine flame ion and stems from hydration of Mg^+ during sampling cooling. When this hydrate signal is added to that of Mg^+, the values in line (d) of Table 7 are obtained, in much better agreement with those in lines (a) and (b); the effect on $\%[Mg^+]$ is shown below line (d). Finally, it is reasonable to believe that some part of the $MgOH_2^+$ signal does, in fact, represent a genuine flame ion produced as protonated MgOH, a major neutral species. If, arbitrarily, 90% of the $MgOH_2^+$ peak height is added to that of Mg^+ and 10% is added to the $MgH_mO_n^+$ signal the values of k_{rec} in line (e) are obtained, with corresponding values of $\%[Mg^+]$ given underneath. The agreement of line (e) with lines (a) and (b) is still

Table 7
Global recombination coefficients k_{rec} of magnesium ions with electrons in fuel-rich H_2–O_2–N_2 flames

Flame number/ k_{rec} (10^{-8} cm^3 molecule^{-1} s^{-1})	2	25	3	4	5
(a) Experimental k_{rec}, run no. 1	2.98	3.67	3.02	2.52	3.60
(b) Experimental k_{rec}, run no. 2	3.10	3.65	3.17	2.82	3.71
(c) Calculated k_{rec}, [Mg^+] from mass spectrum	4.23	4.54	4.73	5.47	7.01
k_{15} (10^{-27} cm^6 molecule^{-2} s^{-1})	1.67	1.79	1.92	2.02	2.20
%[Mg^+]	80.9	79.6	79.0	75.4	67.9
(d) Calculated k_{rec}, [Mg^+] includes [$MgOH_2^+$]	2.94	2.73	2.36	2.42	3.74
%[Mg^+]	87.5	88.9	93.8	91.3	85.0
(e) Calculated k_{rec}, [Mg^+] includes 0.9[$MgOH_2^+$]	3.09	3.28	2.66	2.71	3.94
%[Mg^+]	86.8	88.0	92.3	89.7	83.3

better. The magnitudes are very comparable, and the seemingly erratic temperature dependence is approximately reproduced. In summary, the overall recombination of magnesium flame ions is consistent with accepted recombination coefficients $k_{15} = (4 \pm 2) \times 10^{-24}$ T^{-1} cm^6 molecule^{-2} s^{-1} for Mg^+ and $k_{16} = (2 \pm 1) \times 10^{-7}$ cm^3 molecule^{-1} s^{-1} for the molecular magnesium ions $MgH_mO_n^+$. The rather conservative error limits of ±50% which have been placed on these recombination coefficients encompass the full variation of the values given in Table 7.

4.7. Chemi-ionization of magnesium in flames

It is possible at this stage to consider the chemi-ionization of magnesium by reactions (13) and (14), similar to those which have been measured for Ca, Sr [4], and Ba [5], although the reactions for magnesium are a good deal more endothermic. With the assumption of detailed balance, values of the rate coefficients for chemi-ionization can be calculated from $k_{13} = K_{13}k_{-13}$ and $k_{14} = K_{14}k_{-14}$ with $k_{-13} = k_{-14} = k_{16} = 2 \times 10^{-7}$ cm^3 molecule^{-1} s^{-1}. The equilibrium constants K_{13} and K_{14} were determined by statistical calculations of the relevant free energy functions using Table 2 with $\Delta H_0^0(13)$ and $\Delta H_0^0(14)$ from Table 4 and supplementary data from the JANAF Tables [15]. Values were calculated at the five flame temperatures in the range 1820–2400 K, and are plotted in Fig. 11 as ln K versus $1/T$. Very good straight lines were fitted by least squares to the plots, and give $K_{13} = 0.024\ 16\ \exp(-55\ 700/T)$ and $K_{14} = 0.016\ 71\ \exp(-32\ 970/T)$. These lead to the calculated rate coefficients for chemi-ionization $k_{13} = 4.832 \times 10^{-9}\ \exp(-55\ 700/T)$ and $k_{14} = 3.341 \times 10^{-9}\ \exp(-32\ 970/T)$ cm^3 molecule^{-1} s^{-1}, plotted in Fig. 12 as ln k versus $1/T$. For the five fuel-rich flames in the temperature range 1820–2400 K, $k_{13} = 2.5 \times 10^{-22}$ to 4.1×10^{-19} and $k_{14} = 4.6 \times 10^{-17}$ to 3.7×10^{-15} cm^3 molecule^{-1} s^{-1}, respectively. Using data from Table 6, the relative rates R of reactions (13) and (14) yield $R_{13}/R_{14} =$ 0.98, 0.95, 0.99, 0.95, and 1.02 with increasing temperature for flames 5, 4, 3, 25, and 2, respectively.

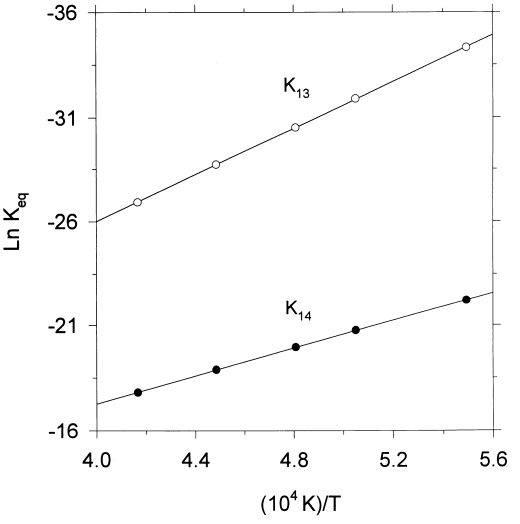

Fig. 11. Van't Hoff plots for the equilibrium constants of the magnesium chemi-ionization reactions (13) and (14) calculated for the five flame temperatures in the range 1820–2400 K.

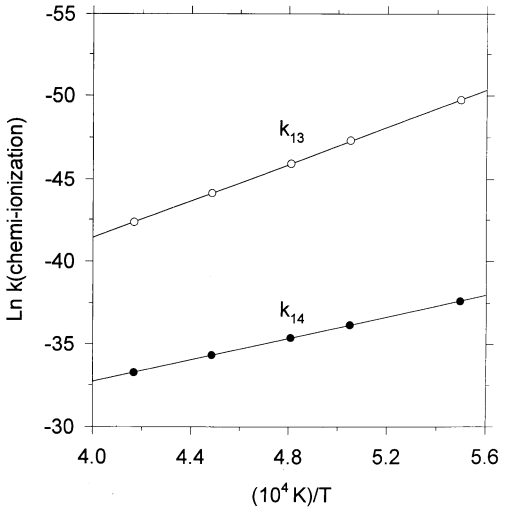

Fig. 12. Linear plots of ln k vs. $1/T$ for the rate constants of the magnesium chemi-ionization reactions (13) and (14) for the five flame temperatures in the range 1820–2400 K.

The near equivalence of the two rates is surprising, given that the rate coefficients are so different; they are compensated by the relative concentrations of the neutral species. Moreover, the values of R_{13} and R_{14} are very close to the value of R_5, the chemi-ionization reaction which produces the natural H_3O^+ ion in these flames. That last statement has to be qualified because it has been assumed that the disequilibrium parameter $\gamma = 1$. Upstream near the reaction zone, Reaction (5) has a γ^3 dependence and is dominant over Reactions (13) and (14). Thus, the experimental observation of the chemi-ionization of magnesium is borderline in our experiments and would be very difficult to detect. This prediction is consistent with the values of k_{13} and k_{14} for Mg which are small compared with their counterparts for Ca, Sr, and Ba.

4.8. Influence of acetate

When these flames were doped with magnesium by spraying aqueous solutions of $MgAc_2.4H_2O$ from the atomizer, the TPI signal increased causing us to believe initially that chemi-ionization of Mg was being observed. Two considerations argue against this hypothesis. First, the steady-state TPI signal observed is a balance of ion production versus ion loss; when molecular ions are replaced by atomic Mg^+ with its slow rate of recombination, the steady-state signal will increase. Second, the nonmetallic acetate part of the salt (Ac = CH_3COO) contains CH_3, introduced into the flame as $\sim 10^{-6}$ mol fraction for a 0.1 M solution. But hydrocarbons ionize very readily in flames by the well-known chemi-ionization reaction $CH + O \rightarrow HCO^+ + e^-$ with rapid conversion to H_3O^+ by the proton transfer reaction $HCO^+ + H_2O \rightarrow H_3O^+ + CO$; this is the basis of the flame ionization detector.

To ascertain whether the acetate addition was contributing to the TPI signal, a 0.1 M solution of acetic acid was sprayed into the flame with the atomizer. Unfortunately, the acetic acid contained a good deal of dissolved potassium giving a large K^+ signal, and the result was inconclusive. Next, a 0.1 M aqueous solution of $MgCl_2.6H_2O$ was sprayed with the atomizer but, again, a definitive result was masked by the presence of potassium impurity in the salt sample. Finally, a 0.1 M solution of $ZnAc_2$ was sprayed with the atomizer; it was known from previous work [54] that Zn does not produce any ions in these flames. The mass spectrum was free of K^+ interference, and a conclusive result was achieved. The TPI signal consisting of natural H_3O^+ ions approximately doubled in each flame tested (flames 3, 4, and 5) when the $ZnAc_2$ solution was sprayed; it is well-established that spraying pure distilled water with the atomizer does not alter the TPI signal. In conclusion, no experimental evidence has been found for the chemi-ionization of magnesium in these flames. The TPI signal increase observed when $MgAc_2.4H_2O$ solution was sprayed by the atomizer is attributable to the two reasons outlined above: namely, decreased ion loss when abundant Mg^+ is present, and chemi-ionization of hydrocarbon from the acetate.

5. Conclusions

Over the past 40 years, many investigations of the gas-phase chemistry of magnesium in the presence of oxygen and hydrogen have produced a variety of scattered thermochemical values. For both the neutral

and the ionic chemistries, most of the values obtained for bond dissociation energies, ionization energies, proton affinities, and the associated standard enthalpies of formation cover a wide range. In an attempt to resolve some of these discrepancies, two lines of approach were pursued in this work, one theoretical by ab initio calculations and the other experimental involving flame–ion mass spectrometry. At the present time, the reliability of high-level calculations for an atom of low atomic number such as Mg has improved to the point where uncertainties of ± 12.6 kJ mol^{-1} *(± 3 kcal mol^{-1})* are usually attainable. The calculations were used to determine the standard enthalpies of formation given in Table 4 for the full range of fairly simple neutral and ionic species encompassing magnesium oxide, hydroxides and hydrates. These form the basis from which the thermochemical values given in Table 5 were derived. It is striking in Table 5 that our calculated values show good agreement in virtually every case with at least one of the literature values, most of which are experimental but some theoretical. Under normal circumstances, a (good) experimental value might be favoured over a calculated one. In the present situation, however, the same types of calculation applied to the full range of magnesium species augers very well for a consistent set of values. For this reason, we are recommending the values in Table 3 obtained from the most sophisticated coupled cluster (CCSD) calculations.

The experimental results from flame–ion mass spectrometry both corroborate and augment the calculated results, and add a further dimension by way of chemical kinetics. Clearly, the flame experiments rely on the calculated values to provide the relative concentrations of the magnesium neutral species in the flames. It was then possible to show that the interconversion of Mg^+ and $MgOH^+$ involves the three-body association of Mg^+ with OH rather than the two-body reaction with H_2O in accordance with the Sugden criterion in flames [11]. Because it was possible to bring $MgOH^+$ and Mg^+ into equilibrium with H_3O^+ within the time scale of the flames, a value of the proton affinity $PA^0_{298}(MgO) = 1056 \pm 29$ kJ mol^{-1} *(252 ± 7 kcal mol^{-1})* could be obtained, in reasonable agreement with both the calculated value in Table 5 and the experimental determination by Freiser's group [9]. Approximate values were also measured for $PA^0_{298}(MgOH) = 919.1$ kJ mol^{-1} *(219.7 kcal mol^{-1})* and $PA^0_{298}[Mg(OH)_2] = 878.2$ kJ mol^{-1} *(209.9 kcal mol^{-1})* which had not been measured previously. The magnitudes are in quite good agreement with the calculated values in Table 5 given the experimental difficulties involved. In this and other cases, the corrections of our experimental values at an average flame temperature of 2100 K to room temperature by statistical mechanical calculations are not large. The recombination of magnesium ions with free electrons could not be measured directly but reasonable values of the recombination coefficients for both atomic Mg^+ and molecular $MgH_mO_n^+$ ions were arrived at by a modeling approach. It was also possible to arrive at values for the rate constants for the pair of chemi-ionization reactions involving Mg + OH and MgO + H. Because the reactions are very endothermic, the rate constants have small magnitudes in comparison with those for the other alkaline earth metals Ca, Sr, and Ba; the direct observation of these reactions in flames is borderline at best. Finally, it was shown that the hydrocarbon present in an acetate salt of a metal, introduced into flames at a concentration of only 10^{-6} mol fraction, is sufficient to produce measureable chemi-ionization.

Acknowledgement

Support of this work by the Natural Sciences and Engineering Research Council of Canada is gratefully acknowledged by three of the authors (J.M.G., A.C.H., and D.K.B.).

References

[1] T.M. Sugden, R.C. Wheeler, Discuss. Faraday Soc. 19 (1955) 76.
[2] K. Schofield, T.M. Sugden, Tenth Symposium (International) on Combustion, Academic, New York, 1965, p. 589.
[3] A.N. Hayhurst, D.B. Kittelson, Proc. R. Soc. London, Ser. A 338 (1974) 155.
[4] A.N. Hayhurst, D.B. Kittelson, Proc. R. Soc. London, Ser. A 338 (1974) 175.
[5] J.M. Goodings, P.M. Patterson, A.N. Hayhurst, J. Chem. Soc. Faraday Trans. 91 (1995) 2257.

[6] J.M. Goodings, S.M. Graham, Int. J. Mass Spectrom. Ion Processes 56 (1984) 193.
[7] D.H. Cotton, D.R. Jenkins, Trans. Faraday Soc. 64 (1968) 2988.
[8] E.P. Hunter, S.G. Lias, NIST Standard Data Base Number 69—March 1998 Release, http://webbook.nist.gov/chemistry/pa-ser.htm.
[9] L. Operti, E.C. Tews, T.J. MacMahon, B.S. Freiser, J. Am. Chem. Soc. 111 (1989) 9152.
[10] E. Murad, J. Chem. Phys. 75 (1981) 4080.
[11] T.M. Sugden, Trans. Faraday Soc. 52 (1956) 1465.
[12] D.E. Jensen, Combust. Flame 18 (1972) 217.
[13] S.D.T. Axford, A.N. Hayhurst, Proc. R. Soc. London, Ser. A 452 (1996) 1035.
[14] C.J. Butler, A.N. Hayhurst, J. Chem. Soc., Faraday Trans. 93 (1997) 1497.
[15] M.W. Chase, Jr., C.A. Davies, J.R. Downey, Jr., D.J. Frurip, R.A. McDonald, A.N. Syverud, JANAF Thermochemical Tables, 3rd ed., J. Phys. Chem. Ref. Data 14 (1985) (Suppl. 1).
[16] J.W. Hastie, D.W. Bonnell, E.R. Plante, High Temp. Sci. 13 (1980) 257.
[17] E.M. Bulewicz, T.M. Sugden, Trans. Faraday Soc. 55 (1959) 720.
[18] M.J. Frisch, G.W. Trucks, H.B. Schlegel, P.M.W. Gill, B.G. Johnson, M.A. Robb, J.R. Cheeseman, T. Keith, G.A. Petersson, J.A. Montgomery, K. Raghavachari, M.A. Al-Laham, V.G. Zakrzewski, J.V. Ortiz, J.B. Foresman, J. Cioslowski, B.B. Stefanov, A. Nanayakkara, M. Challacombe, C.Y. Peng, P.Y. Ayala, W. Chen, M.W. Wong, J.L. Andres, E.S. Replogle, R. Gomperts, R.L. Martin, D.J. Fox, J.S. Binkley, D.J. DeFrees, J. Baker, J.P. Stewart, M. Head-Gordon, C. Gonzalez, J.A. Pople, GAUSSIAN 94, Revision B.2, Gaussian, Inc., Pittsburgh, PA, 1995.
[19] P. Pulay, Mol. Phys. 17 (1969) 197.
[20] (a) H.B. Schegel, S. Wolfe, F. Bernardi, J. Chem. Phys. 63 (1975) 3632; (b) H.B. Schegel, J. Comput. Chem. 3 (1982) 214.
[21] J.S. Binkley, J.A. Pople, Int. J. Quantum Chem. 9 (1975) 229.
[22] R. Krishnan, M.J. Frisch, J.A. Pople, J. Chem. Phys. 72 (1980) 4244.
[23] A.D. McLean, G.S. Chandler, J. Chem. Phys. 72 (1980) 5639.
[24] P.C. Hariharan, J.A. Pople, Chem. Phys. Lett. 66 (1972) 217.
[25] M.M. Francl, W.J. Pietro, W.J. Hehre, J.S. Binkley, M.S. Gordon, D.J. DeFrees, J.A. Pople, J. Chem. Phys. 77 (1982) 3654.
[26] J. Chandrasekhar, J.G. Andrade, P.v.R. Schleyer, J. Am. Chem. Soc. 103 (1981) 5609.
[27] T. Clark, J. Chandrasekhar, G.W. Spitznagel, P.v.R. Schleyer, J. Comput. Chem. 4 (1983) 294.
[28] C.F. Rodriquez, Ph.D. Dissertation, York University, Toronto, 1994.
[29] J.A. Pople, M. Head-Gordon, K. Raghavachari, J. Chem. Phys. 87 (1987) 5968.
[30] M.J. Frisch, J.A. Pople, J.S. Binkley, J. Chem. Phys. 80 (1984) 3265.
[31] J. Cizek, Adv. Chem. Phys. 14 (1969) 35.
[32] G.D. Purvis, R.J. Bartlett, J. Chem. Phys. 76 (1982) 1910.
[33] G.E. Scuseria, C.L. Janssen, H.F. Schaefer III, J. Chem. Phys. 89 (1988) 7382.
[34] G.E. Scuseria, H.F. Schaefer III, J. Chem. Phys. 90 (1989) 3700.
[35] S.G. Lias, J.E. Bartmess, J.F. Liebman, J.L. Holmes, R.D. Levin, W.G. Mallard, J. Phys. Chem. Ref. Data 17 (1988) (Suppl. 1).
[36] C.F. Rodriquez, A.C. Hopkinson, Can. J. Chem. 70 (1992) 2234.
[37] C.F. Rodriquez, D.K. Bohme, A.C. Hopkinson, J. Am. Chem. Soc. 115 (1993) 3263.
[38] C.F. Rodriquez, A.C. Hopkinson, D.K. Bohme, J. Phys. Chem. 100 (1996) 2942.
[39] A.E. Ketvirtis, D.K. Bohme, A.C. Hopkinson, J. Phys. Chem. 99 (1995) 16121.
[40] C.E. Moore, Natl. Stand. Ref. Data Ser., U.S. Nat. Bur. Stand., NSRDS-NBS 34, Superintendent of Documents, U.S. Government Printing Office, Washington, DC, 1970.
[41] J.B. Pedley, E.M. Marshall, J. Phys. Chem. Ref. Data 12 (1983) 967.
[42] K. Schofield, in Gas-Phase Metal Reactions, A. Fontijn (Ed.), North-Holland, Amsterdam, 1992, p. 542.
[43] C.W. Bauschlicher Jr., H. Partridge, Chem. Phys. Lett. 205 (1993) 479.
[44] I. García Questa, A. Sánchez de Merás, I. Nebot Gil, Chem. Phys. Lett. 205 (1993) 484.
[45] K.P. Huber, G. Herzberg, Molecular Spectra and Molecular Structure. IV. Constants of Diatomic Molecules, Van Nostrand Reinhold, New York, 1979.
[46] D.H. Cotton, D.R. Jenkins, Trans. Faraday Soc. 65 (1969) 376.
[47] M. Sodupe, C.W. Bauschlicher Jr., Chem. Phys. Lett. 195 (1992) 494.
[48] C.W. Bauschlicher Jr., M. Sodupe, H. Partridge, J. Phys. Chem. 96 (1992) 4453.
[49] C.S. Yeh, K.F. Willey, D.L. Robbins, J.S. Pilgrim, M.A. Duncan, Chem. Phys. Lett. 196 (1992) 233.
[50] H. Watanabe, S. Iwata, K. Hashimoto, F. Misaizu, K. Fuke, J. Am. Chem. Soc. 117 (1995) 755.
[51] F. Misaizu, M. Sanekata, K. Fuke, S. Iwata, J. Chem. Phys. 100 (1994) 1161.
[52] J.M. Goodings, C.S. Hassanali, P.M. Patterson, C. Chow, Int. J. Mass Spectrom. Ion Processes 132 (1994) 83.
[53] J.M. Goodings, S.M. Graham, W.J. Megaw, J. Aerosol Sci. 14 (1983) 679.
[54] Q Tran, N.S. Karellas, J.M. Goodings, Can. J. Chem. 66 (1988) 2210.
[55] J.M. Goodings, P.M. Patterson, Int. J. Mass Spectrom. Ion Processes 151 (1995) 17.
[56] J.M. Goodings, Q.F. Chen, Can. J. Chem (1998) 1437.
[57] A.N. Hayhurst, D.B. Kittelson, N.R. Telford, Combust. Flame 28 (1977) 123.
[58] A.N. Hayhurst, D.B. Kittelson, Combust. Flame 28 (1977) 137.
[59] N.A. Burdett, A.N. Hayhurst, Combust. Flame 34 (1979) 119.
[60] D.R. Lide (Ed.), CRC Handbook of Chemistry and Physics, 73rd ed., CRC, Boca Raton, FL, 1992.
[61] S.D.T. Axford, A.N. Hayhurst, J. Chem. Soc. Faraday Trans. 91 (1995) 827.
[62] A.N. Hayhurst, N.R. Telford, J. Chem. Soc., Faraday Trans. 1 71 (1975) 1352.
[63] A.N. Hayhurst, Department of Chemical Engineering, University of Cambridge, UK, personal communication.
[64] A.F. Ashton, A.N. Hayhurst, Combust. Flame 21 (1973) 69.